Check for updates

Two Ln-based metal–organic frameworks based on the 5-(1H-1,2,4-triazol-1-yl)-1,3-benzenedicarboxylic acid ligand: syntheses, structures, and photocatalytic properties†

Fei Yuan, [iD] [a] Chunmei Yuan, [a] Baoyue Cao, [a] Youying Di, [a] Shumin Wang, *[a] Mingbao Liu, [a] Abhinav Kumar, [iD] *[b] Chuncheng Shi*[c] and Mohd. Muddassir [iD] [d]

Two new metal–organic frameworks (MOFs) having the formula $[Ln_2(H_2O)_3(L)_3 \cdot 3H_2O]_n$ (Ln = Sm for **MOF-Sm** and Tb for **MOF-Tb**) have been synthesized solvothermally by reacting $LnCl_3 \cdot 6H_2O$ with 5-(1H-1,2,4-triazol-1-yl)-1,3-benzenedicarboxylic acid (H_2L) and characterized. Single crystal X-ray analyses for **MOF-Sm** and **MOF-Tb** revealed that both MOFs are isostructural and display a (6,8)-connected 3D structure with a point symbol of $(3^5 \cdot 4^4 \cdot 6^6)(3^5 \cdot 4^6 \cdot 5^{17})$. The natures of weak interactions existing in both MOFs have been assessed using Hirshfeld surface analyses and fingerprint plots. The utility of **MOF-Sm** as a photocatalyst for the safe photodegradation of the model aromatic dye methyl violet (MV) is also checked. The photocatalysis results showed that **MOF-Sm** offers reasonable photocatalytic degradation of this dye. The plausible photocatalytic mechanism of **MOF-Sm** aided photocatalysis has been explained with the help of band gap calculations using density of states (DOS) and partial DOS plots.

Introduction

The use of photocatalytic methods for degradation of aromatic pollutants have been explored extensively due to their simple operation, low energy consumption and high efficiency.[1–3] Compared to traditional photocatalysts *viz.* traditional semi-conductors (such as TiO_2 and some metal sulphides), metal–organic frameworks (MOFs) have comprehensively been used in catalysis to treat organic pollutants in wastewater. This is because of their potential semiconducting properties which they exhibit on exposure to light.[4,5] It has now been established that the structure of the resultant architecture in MOFs is usually affected by several factors *viz.* selection of a suitable ligand, metal cations, solvent, temperature, heating as well as cooling rate, *etc.* But amongst these pertinent factors, the apt selection of suitable organic linkers is considered as a sensible

way to fabricate the desirable MOFs.[6,7] The previous reports suggest that the imidazole-carboxylate bi-functional ligands offer some advantages for designing and fabrication of targeted MOFs. This is because, this ligand possess several coordination sites to meet the coordination requirements of metal ions.[8,9]

The photocatalysis technology utilizing solar light has now been considered as one of the most effective technology for waste water treatment due to its various advantages, such as low cost, requiring low energy and better efficiency. The irradiation of UV-visible light can induce the excitation of electrons in dye molecules. The excited states of [dye]* can have stronger inter-actions with the active sites of MOF and hence results in more surface adsorption. Under UV light, the photo-excited [dye]* gets degraded by ·OH radicals which is generated *via* direct excitation pathway by MOFs.[10] Methyl violet (MV) is a typical cationic dye that is widely used in paper making, spraying and textile industries. Moreover, MV can affect human's physical health and can cause vomiting, shock, jaundice and cyanosis. This is because this dye can interact freely with the negatively charged membrane surface of cells, and then can reach cell's nucleus.[10b] Therefore, there is an utmost need to explore safe and sustainable treatment methods to degrade such aromatic dyes to convert them to relatively less harmful products.

Mostly transition metals mainly belonging to 3d transition series have been utilized to develop MOFs having varied archi-tectures which eventually have been utilised as photocatalysts working under UV-vis irradiation.[4–6] However, lanthanide based-MOFs which although possess enormous potential have

[a]Shaanxi Key Laboratory of Comprehensive Utilization of Tailings Resources, College of Chemical Engineering and Modern Materials, Shangluo University, Shangluo 726000, China. E-mail: slyuanf@126.com; happywshm@126.com
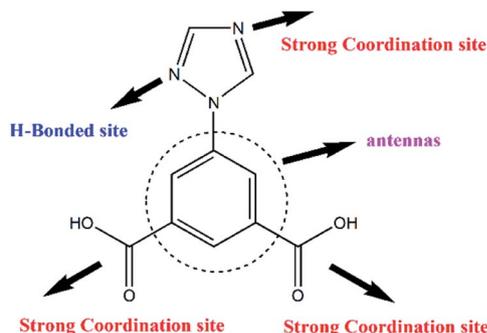
[b]Department of Chemistry, Faculty of Science, University of Lucknow, Lucknow, 226007, India. E-mail: abhinavmarshal@gmail.com

[c]Department of Pharmacy, School of Medicine, Xi'an International University, Xi'an, 710077, Shaanxi, China. E-mail: shichch66xaiuedu@163.com

[d]Department of Chemistry, College of Sciences, King Saud University, Riyadh 11451, Saudi Arabia

Scheme 1 Chemical structure of 5-(1H-1,2,4-triazol-1-yl)-1,3-benzenedicarboxylic acid (H₂L) showing different coordination and hydrogen bonding sites.

not been explored exhaustively as photocatalyst to photodegrade pollutants especially the aromatic dyes present in the wastewater discharge.

Hence, in view of aforementioned points and in the pursuit of new lanthanide based MOFs bi-functional imidazole-carboxylate ligand a multifunctional ligand, 5-(1H-1,2,4-triazol-1-yl)-1,3-benzenedicarboxylic acid (H₂L)[11] have been selected in the presented study. The selection of this ligand is to increase the coordination function and possible synergism of the two functional groups, as the triangular linker. The H₂L linker has been designed because of the following merits (Scheme 1). (1) The aromatic carboxylate and triazole ligands are two very important moieties utilized for the construction of MOFs due to their versatile coordinated modes.[12] (2) The aromatic fragments can be regarded as antenna which increases light absorption and transfer energy to metal efficiently through "antenna effect".[13] With these view points, in the presented work two new isostructural MOFs having general formula [Ln₂(H₂O)₃(L)₃·3H₂O]ₙ (Ln = Sm for **MOF-Sm** and Tb for **MOF-Tb**), have been synthesized hydrothermally and characterized. In addition to molecular structure investigation of both MOFs their Hirshfeld surface analyses have been executed. The **MOF-Sm** has further been employed as possible photocatalyst for photodegradation of a model organic dye methyl violet. These results of all these studies are presented herewith.

Experimental

Materials and methods

These 5-(1H-1,2,4-triazol-1-yl)-1,3-benzenedicarboxylic acid (H₂L) and LnCl₃ materials were purchased from Jinan Henghua Sci and Tec Co., Ltd and used without further purification. The FTIR spectra were recorded in KBr discs on Nicolet Avatar 360 FTIR spectrometer in the 400–4000 cm⁻¹ region. Powder X-ray diffraction (PXRD) data for the MOFs were recorded on Bruker D8 ADVANCE X-ray powder diffractometer using Cu-Kα radiation of 1.5418 Å.

X-ray crystallography

The single crystal X-ray diffraction data were collected on Bruker SMART APEX diffractometer using graphite monochromated Mo-Kα radiation ($\lambda = 0.71073$ Å) by using an ω-scan technique. The structures were solved by direct method

(SHLEXS-2014) and refined using the full-matrix least-square procedure based on F^2 (Shelxl-2014).[14] All the hydrogen atoms were generated geometrically and refined isotropically using a riding model. All non-hydrogen atoms were refined with anisotropic displacement parameters. Crystallographic details and selected bond dimensions for **MOF-Sm** and **MOF-Tb** are listed in Tables S1 and S2,† respectively. CCDC no.: 2014162 and 2014163.†

Photocatalytic method

The finally divided sample of **MOF-Sm** (40 mg) was dispersed in 50 mL aqueous solution of methyl violet (MV) having concentration of 10 mg L⁻¹. After adding the MOF, the mixture was stirred under dark for 30 min to ensure the establishment of adsorption–desorption equilibrium. After that, the photocatalytic degradation of MV was conducted using XPA-7 type photochemical reactor fitted with 100 W mercury lamp (mean wavelength 365 nm) having light intensity of 12.7 mW cm⁻² at quartz tube positions. During the photocatalytic degradation, aliquots of 5.0 mL were isolated at specific time intervals and separated through centrifugation and then subsequently the intensity of characteristic electronic absorption band of MV recorded using UV-visible spectrophotometer. In addition, a control experiment was conducted under the similar reaction conditions but without the addition of **MOF-Sm**.

Computational details

The possible photocatalytic mechanism by which the **MOF-Sm** performed the photodegradation of the MV have been explained with the aid of theoretical band gap calculations. The smallest unit of this MOF was geometry optimized using the B3LYP functional,[15a,15b] using 6-31G** basis set for all the atoms except Sm for which SDDALL basis set was employed. All the calculations were performed using Gaussian 09 program.[15c] The final results of the calculations were used to construct the density of states (DOS) and fragmented partial DOS plots using GaussSum 3.1 version of programs.[15d]

Hirshfeld surface analyses

Molecular Hirshfeld surfaces[16–23] in the crystal structures of both MOFs were constructed by using the procedure mentioned previously.[24]

Synthesis of [Sm₂(H₂O)₃(L)₃·3H₂O]ₙ (MOF-Sm)

To the 10 mL aqueous solution of SmCl₃·6H₂O (0.0382 g, 0.1 mmol), ligand H₂L (0.0233 g, 0.1 mmol) was added and the mixture was stirred for 30 min. Thereafter the pH of this mixture was adjusted to 6.0 by adding aqueous solution of 0.5 M NaOH. The obtained mixture was transferred to a Teflon-lined stainless steel vessel (25 mL), sealed and heated to 160 °C for 72 h. After 72 h the vessel was cooled to room temperature at a rate of 5 °C h⁻¹. The colourless block crystals of **MOF-Sm** were obtained which was washed with distilled water (5 mL), yield 28.8% based on H₂L. IR (cm⁻¹): 3486(vs); 3128(m); 2366(m);

1632(v); 1583(v); 1444(vs); 1388(v); 1219(w); 1134(m); 1076(m); 785(v); 729(v); 663(m).

Synthesis of $[Tb_2(H_2O)_3(L)_3 \cdot 3H_2O]_n$ (MOF-Tb)

The solvothermal reaction adopted for the synthesis of **MOF-Tb** was similar to that used for **MOF-Sm**, except that $TbCl_3 \cdot 6H_2O$ (0.0373 g, 0.1 mmol) was used in the reaction. The faint yellow block crystals of **MOF-Tb** were obtained which was washed with distilled water (5 mL), yield 49.8% based on H_2L. IR (cm^{-1}): 3468(vs); 3129(m); 1632(v); 1583(v); 1448(vs); 1388(v); 1219(m); 1134(m); 1067(m); 785(v), 730(v), 672(v).

Results and discussion

Molecular structure description

X-ray single crystal structural analysis reveals that **MOF-Sm** and **MOF-Tb** crystallize in the triclinic system with $P\bar{1}$ space group and possess isostructural 3D network. Here, we select **MOF-Sm** as a representative example for a detailed discussion of the structure. As illustrated in Fig. S1,† the asymmetric unit of **MOF-Sm** contains two independent Sm(III) ions, three L^{2-} ligands, three coordinated water molecules and three lattice water molecules.

Two kinds of L^{2-} are existing in **MOF-Sm**. In addition to type-a L^{2-} (Fig. 1a), type-b L^{2-} is also present which through one of its triazole nitrogen and two carboxylates is participating in the formation of self-assembly framework (Fig. 1b).[25] The MOF comprises of two different kinds of secondary building units (SBU). The first type of SBU consists of two nine-coordinated Sm(III) and surrounded by two oxygen atoms from two terminal H_2O, two nitrogen atoms from two trizaole groups and twelve oxygen atoms from six carboxylate groups (Fig. 1c). While in second type of SBU, the nitrogen atoms are replaced by two oxygen atoms of two terminal H_2O ligands (Fig. 1d and S2†). In other words, the carboxylate group exhibits bridging μ_2-η^2
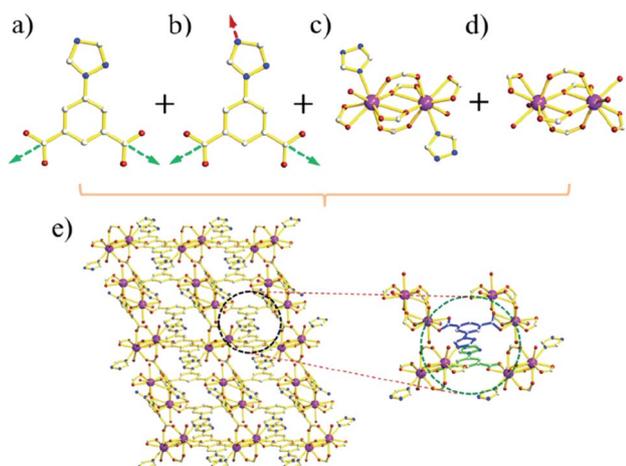

Fig. 1 (a and b) The coordination modes of the two kinds of ligands in **MOF-Sm**; (c and d) two kinds of SBUs in **MOF-Sm**; (e) the packing mode of **MOF-Sm**. Silver, blue, red and purple spheres represent C, N, O and Sm, respectively. Hydrogen atoms have been omitted for clarity.
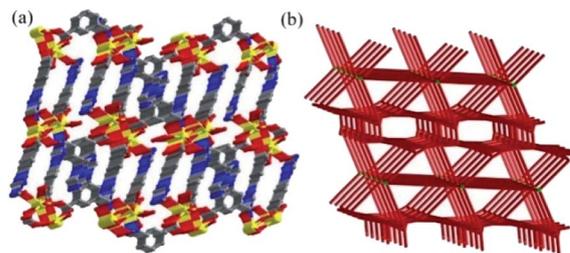

Fig. 2 (a) Perspective view of 3D network in **MOF-Sm**; and (b) schematic representations of 6,8-connected dinuclear metal units coordinated with L^{2-} ligands.

mode in type-a L^{2-} ligand, while two different coordination modes from the pair of carboxylate groups of type-b L^{2-} ligand can be seen which coordinates to Sm(III) in μ_1-η^2 and μ_2-η^2:η^1 modes.[26]

Each SBU connects adjacent SBU through two kinds of L^{2-} bridges in four different directions which forms an unusual three-dimensional network with one-dimensional channels of *ca.* 5.2 Å × 6.3 Å (Fig. 1e and 2a). Topologically, each SBU can be simplified as nodes and the L^{2-} ligands can be considered as 2-connected and 3-connected nodes, the complicated architecture of **MOF-Sm** is simplified to a new (6,8)-connected 3D network with a point symbol of $(3^5 \cdot 4^4 \cdot 6^6)(3^5 \cdot 4^6 \cdot 5^{17})$ as analysed by the TOPOS program (Fig. 2b).[27] Moreover, the $\pi \cdots \pi$ stacking interactions between the trizaole rings of two kinds of L^{2-} ligands (centroid-to-centroid distances of 3.86(3) Å) were observed in the channel (Fig. 1e). The water molecules and uncoordinated imidazole groups occupy the voids of three-dimensional network. The solvent accessible volume in **MOF-Sm** calculated excluding water molecules by PLATON analysis is 6.5% of the cell volume. Wang *et al.* have reported four water-stable lanthanide metal–organic frameworks (Ln(III)-MOFs) (**1**-Ln, Ln(III) = Tb, Eu, Dy, and Sm), $[Ln(L)(HL)(H_2O)_2]$ (H_2L = 4-(1H-1,2,4-triazol-1-yl)isophthalic acid), where the deprotonated H_2L ligands have two different coordination modes. These adjacent SBUs were linked with L^{2-} linkers to give a 2D layer along the *c* direction. Furthermore, these C8–H8A···N3 (1.935 Å) hydrogen bonds exist between the neighbouring
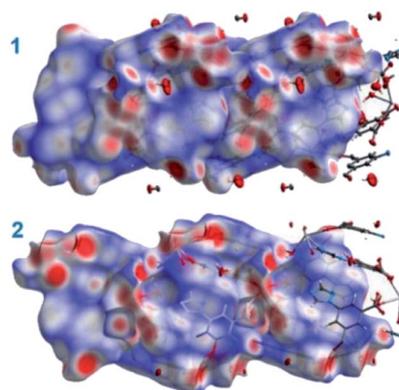

Fig. 3 The d_{norm} surfaces for **MOF-Sm** and **MOF-Tb**.

layers, extending the 2D network into a 3D framework. Topologically, these structures could be viewed as a binodal (3,4)-connected topological net with a point symbol of $(4^2 \cdot 6^3 \cdot 8)(4^2 \cdots 6)$.[13b] The difference in structures is due to the isomerism of the functional groups of the ligands.

Hirshfeld surface analyses

The Hirshfeld surfaces for both the MOFs are shown in Fig. 3. The dominant interactions are revealed by circular depressions in the d_{norm} plots which have been constructed between −0.7 to 1.4 Å. The weak interactions are shown effectively in d_{norm} surfaces with large circular depressions (deep red), suggesting the existence of strong interactions. While, the longer and weaker interactions are shown as small areas in the Hirshfeld surface plots.

In fingerprint plots for both MOFs (Fig. 4), the complementary regions are visible where one molecule behaves as a donor ($d_e > d_i$) whilst another acts as an acceptor ($d_e < d_i$). In addition, the characteristic plots could be split apart to specify the atom pairs having close contacts. This enables us to evaluate the contributions by the different strong as well as weak interactions present in the structure. In the complex the O···H/H···O

and N···H/H···N interactions appear as two distinct spikes of unequal lengths in the 2D fingerprint plots between the region 2.03 Å < ($d_e + d_i$) < 2.47 Å as light sky-blue pattern in full fingerprint 2D plots. While, the π···π non-covalent interactions are lying in the upper middle portion of the fingerprint plot in the region 1.6 Å < ($d_e + d_i$) < 2.4 Å. For **MOF-Sm**, the O···H/H···O, N···H/H···N and π···π interactions contribute 24.5%, 10.8% and 2.8%, respectively. While, in **MOF-Tb** the O···H/H···O, N···H/H···N and π···π interactions contribute 24.3%, 10.6% and 2.6%, respectively to its total Hirshfeld surface. The small variation in different contribution in the fingerprint plots could be ascribed to the isostructural nature of both the MOFs.

IR spectra and thermal properties

In the FTIR spectra of both MOFs (Fig. S3†), the main characteristic bands at ∼1384 cm^{-1} and ∼1631 cm^{-1} are mainly attributed to the asymmetric and symmetric stretching vibrations of the carboxylate groups, respectively. The characteristic absorption band was not observed at 1700 cm^{-1} which suggests the complete deprotonation of H$_2$L ligand.[28] This difference in the vibration magnitudes corresponding to symmetric and asymmetric stretch $\Delta\nu[\nu_{as(COO)} - \nu_{s(COO)}]$ are *ca.* 139 cm^{-1} and 126 cm^{-1} for **MOF-Sm** and **MOF-Tb**, respectively. This indicate bridging bidentate coordination modes of carboxylate groups to the central metal atoms. The bands at 3486 and 3461 cm^{-1} for **MOF-Sm** and **MOF-Tb** respectively, are assigned to the stretching vibrations $\nu_{(OH)}$ of water molecules. The bands at *ca.* 1583 cm^{-1} for both MOFs are assigned to the $\nu_{(C=N)}$ absorption in the imidazole ring of L^{2-} ligand. To assess the thermal stabilities of both MOFs, thermogravimetric analyses (TGA) were performed under nitrogen atmosphere (Fig. S4†). The TGA analyses indicated that the weight loss of 9.8% (calcd 9.6%) in the first step from 57 to 255 °C corresponds to the removal of

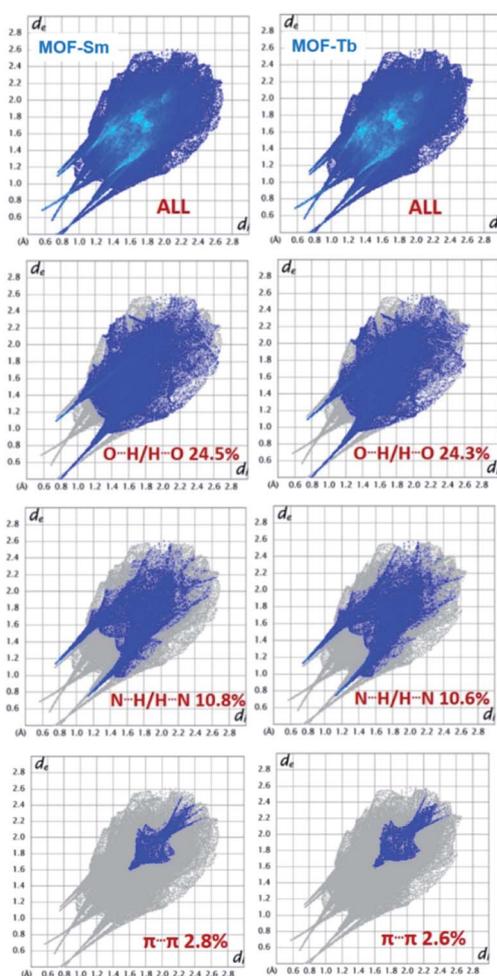**Fig. 4** Fingerprint plots for both the MOFs.
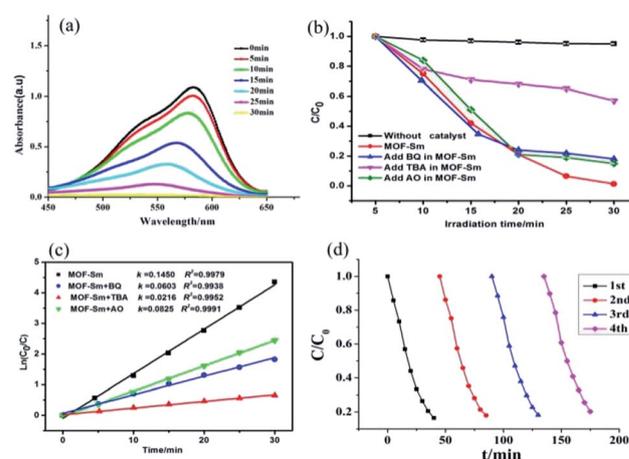

Fig. 5 (a) Absorption spectra of the MV solutions during the decomposition reaction under UV irradiation in presence of **MOF-Sm**; (b) photodegradation of the MV solution with different scavenger solutions in presence of **MOF-Sm**; (c) linear-log plot as a function of visible light irradiation time; (d) cycles of the photocatalytic degradation of MV in **MOF-Sm**.

water molecules. The second weight loss occurred in a temperature range from 342 to 608 °C which corresponded to the decomposition of the L^{2-} ligands which eventually ruptures the MOF framework.

Photocatalytic property

In this work, we employed the photodegradation of MV as a model to demonstrate the photocatalytic activities of **MOF-Sm** under UV light irradiation (Fig. 5). For **MOF-Sm**, about 98.7% degradation of MV was observed after 30 min. Apart for performing the photodegradation of MV in presence of **MOF-Sm**, for the sake of comparison, the control experiment (without the addition of **MOF-Sm**) was also executed. Under control experimental condition, the photodegradation of MV was only 13% within 40 min (Fig. S5†), which indicated that negligible decomposition of the dye without the photocatalyst **MOF-Sm**.[29–31] Also, the change in the C_t/C_0 plot of MV solutions vs. reaction time is presented in Fig. 5b. The distinct variation in photodegradation of MV compared with the control experiment indicates that **MOF-Sm** is an active photocatalyst for the decomposition of MV in the presence of UV irradiation. The photocatalytic performances of several Ln-based MOFs for aromatic dye putrefaction under UV radiation; visible radiation; or both UV and visible light irradiation are listed in Table S3.† This comparison indicates that the photocatalytic performances of MOFs are affected by several factors such as absorption of the light, charge separation efficiency, number as well as the nature of catalytic sites. This suggest that during Ln-based cation used to prepare MOFs, the resulting MOF frameworks, extent of conjugation, coordination environment and steric hindrance around the active metal sites play vital role in deciding the suitability of any MOF to be used as photocatalyst.

In order to gain insight into the nature of active species involved in the dye degradation process, the photocatalytic reactions were performed under the similar conditions using catalyst **MOF-Sm** along with several radical scavengers such as tertiary butyl alcohol (TBA), benzoquinone (BQ) and ammonium oxalate (AO) (Fig. 5b and 6). The radical scavenging experiments demonstrated that the photocatalytic activity of **MOF-Sm** decreased to 47% after 30 min of irradiation and the
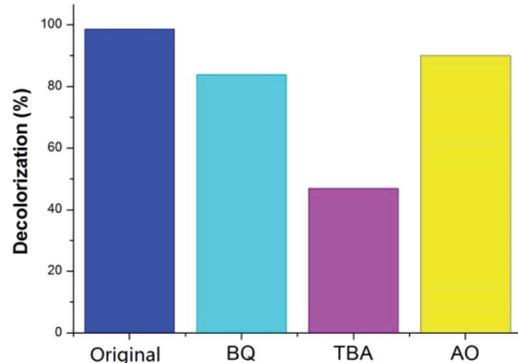
Table 1 The pseudo first-order rate constants and the corresponding square of the correlation coefficients for the photocatalytic degradation reactions

Material	MV	
	k (min^{-1})	R^2
MOF-Sm	0.1450	0.9979
MOF-Sm + BQ	0.0603	0.9938
MOF-Sm + TBA	0.0216	0.9952
MOF-Sm + AO	0.0825	0.9991

degradation rate was 0.0216 min^{-1} when the TBA was added in the system (Fig. 5c and Table 1). However, the degradation of MV by **MOF-Sm** in the presence of other two radical scavengers viz. BQ and OA doesn't declined significantly (Fig. 5b, c and 6).

The degradation mechanism for MV could be explained as follows: the excited photo-electron moves from the valence band (VB) to the conduction band (CB), when **MOF-Sm** is under UV-vis light illumination. Meanwhile, the excited holes in the VB at the Sm(III) sites helps to produces hydroxyl radicals which decomposes the organic pollutants (Scheme 2). Thus, hydroxyl radicals play an important role in degrading different organic dyes because of its strong oxidising ability in aqueous solution. This mechanism is also found in other Ln-MOFs.[40] Furthermore, when **MOF-Sm** was suspended into the aqueous solution of MV in the dark for two days, no significant decline in the characteristic absorption intensity of MV was observed, which ruled-out the possibility of adsorption of dye molecule into the framework of **MOF-Sm**.[32–36] Hence, this experiment indicates that **MOF-Sm** showed excellent catalytic activity and good stability for the photodegradation of MV in water. To check the photocatalytic ability of the recycled **MOF-Sm**, after each photocatalytic cycle of MV, the photocatalyst **MOF-Sm** was filtered, washed with distilled water under stirring, and then filtered again. No significant reduction in percentage photodegradation of MV was observed even when the photocatalyst was used four

Fig. 6 Comparison of the percentage photodegradation of MV solution with different scavenger in presence of **MOF-Sm**.
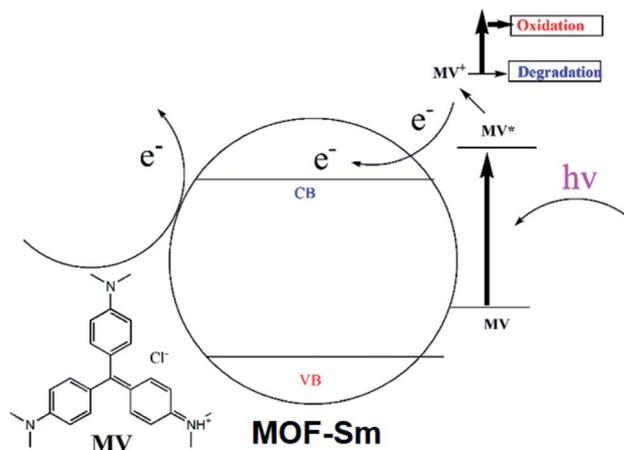
Scheme 2 The possible mechanism involved in dye degradation and electron transfer in photocatalytic process.
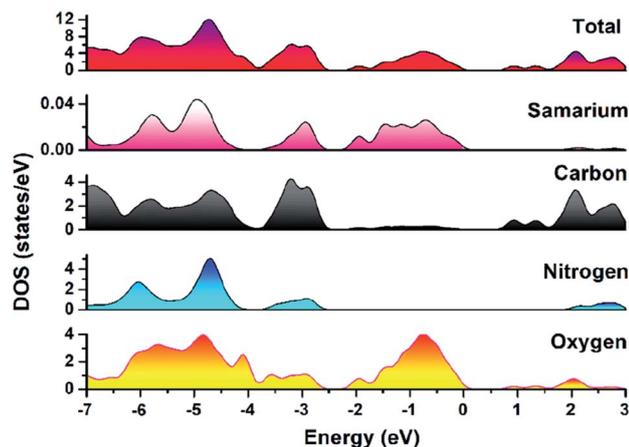
Fig. 7   Density of states (DOS) and partials DOS plots for MOF-Sm.

cycles.[37–39] The result indicated that **MOF-Sm** shows good reproducibility as photocatalyst. Moreover, the recovered sample of **MOF-Sm** was further characterized by powder X-ray diffraction (PXRD) which showed patterns nearly identical to that of the pristine **MOF-Sm** (Fig. S6†). This suggested that the MOF retained its framework integrity after performing photocatalysis of MV.

To explore the mechanism using which **MOF-Sm** performed photo-degradation of MV, the band structure calculations were performed which was based on density functional theory (*vide supra*). The obtained results of this calculation were used to construct DOS and partial DOS plots which are shown in Fig. 7. The plots display that the valence band (VB) in **MOF-Sm** is having major contributions from aromatic carbons and carboxylate oxygen atoms. While Sm(III) and nitrogen centres of traizole offered almost negligible contribution in the VB. Likewise, the conduction band (CB) in **MOF-Sm** is again having contributions from aromatic carbon and oxygen centers. Hence, pDOS plots suggest that in **MOF-Sm**, the electronic transitions are of ligand-to-ligand type. During photo-excitation one L^{2-} transfers electron to another L^{2-} ligand which lead to generation of holes and these holes further assist in the production of hydroxyl radicals by reaction with water. These hydroxyl radicals then perform mineralization of MV.

Conclusion

In summary, we have successfully synthesized and characterized two isostructural Ln-MOFs based on a versatile bifunctional imidazole-carboxylate 5-(1*H*-1,2,4-triazol-1-yl)-1,3-benzenedicarboxylic acid ligand. They exhibit a unique (6,8)-connected network with a point symbol of $(3^5 \cdot 4^4 \cdot 6^6)(3^5 \cdot 4^6 \cdot 5^{17})$. The various interactions existing in the crystal structure of both the MOFs were investigated using Hirshfeld surface analyses and the fingerprint plots obtained during Hirshfeld surface calculations allowed scrutiny of all the important intermolecular interactions within the crystal structures. The photocatalytic results of **MOF-Sm** showed that this material can be suitable for performing photodegradation of MV and analogues

aromatic dyes. This induced photocatalytic properties was ascribed to the formation of hydroxyl radicals generated during the ligand to ligand transitions. The presented work will generate interest amongst inorganic chemistry to design and synthesize newer Ln-based MOF for their use as photocatalyts for the safe and sustainable degradation of organic dyes.

Conflicts of interest

There are no conflicts to declare.

Acknowledgements

References

1 (*a*) M. Zalfani, Z. Y. Hu, W. B. Yu, M. Mahdouani, R. Bourguiga, M. Wu, Y. Li, G. V. Tendeloo, Y. Djaoued and B. L. Su, *Appl. Catal., B*, 2017, **205**, 121–132; (*b*) Q. Liang, M. Zhang, Z. Zhang, C. Liu, S. Xu and Z. Li, *J. Alloys Compd.*, 2017, **690**, 123–130.

2 (*a*) W. Guan, X. Gao, G. Ji, Y. Xing, C. Du and Z. Liu, *J. Solid State Chem.*, 2017, **255**, 150–156; (*b*) V. A. Tran, A. N. Kadam and S.-W. Lee, *J. Alloys Compd.*, 2020, **835**, 155414; (*c*) K. G. Liu, F. Rouhani, X. M. Gao, M. Abbasi-Azad, J. Z. Li, X. D. Hu, W. Wang, M. L. Hu and A. Morsali, *Catal. Sci. Technol.*, 2020, **10**, 757–767.

3 (*a*) M. L. Hu, V. Safarifard, E. Doustkhah, S. Rostamnia, A. Morsali, N. Nouruzi, S. Beheshti and K. Akhbari, *Microporous Mesoporous Mater.*, 2018, **256**, 111–127; (*b*) J.-L. Wang, C. Wang and W. Lin, *ACS Catal.*, 2012, **2**, 2630–2640; (*c*) A. Ma, J. Wu, Y. Han, F. Chen, B. Li, S. Cai, H. Huang, A. Singh, A. Kumar and J. Liu, *Dalton Trans.*, 2018, **47**, 9627–9633.

4 (*a*) Y. Pan, Q. Ding, H. Xu, C. Shi, A. Singh, A. Kumar and J. Liu, *CrystEngComm*, 2019, **21**, 4578–4585; (*b*) Z. Zhang, J. Zhang, T. Wu, X. Bu and P. Feng, *J. Am. Chem. Soc.*, 2008, **130**, 15238–15239; (*c*) J. Cao, Z. Yang, W. Xiong, Y. Zhou, Y. Peng, X. Li, C. Zhou, R. Xu and Y. Zhang, *Chem. Eng. J.*, 2018, **353**, 126–137.

5 (*a*) M. Mon, R. Bruno, J. Ferrando-Soria, D. Armentano and E. Pardo, *J. Mater. Chem. A*, 2018, **6**, 4912–4947; (*b*) Q. Ding, Y. Pan, Y. Luo, M. Zhou, Y. Guan, B. Li,

M. Trivedi, A. Kumar and J. Liu, *ACS Omega*, 2019, **4**, 10775–10783; (*c*) J.-Z. Gu, Y. Cai, M. Wen, Z.-F. Shiand and A. M. Kirillov, *Dalton Trans.*, 2018, **47**, 14327–14339.

6 (*a*) Y.-F. Peng, S. Zhao, K. Li, L. Liu, B.-L. Liand and B. Wu, *CrystEngComm*, 2015, **17**, 2544–2552; (*b*) M. S. Deenadayalan, N. Sharma, P. K. Verma and C. M. Nagaraja, *Inorg. Chem.*, 2016, **55**, 5320–5327; (*c*) M. L. Hu, Y. M. Mohammad and A. Morsali, *Coord. Chem. Rev.*, 2019, **387**, 415–435; (*d*) J. Liu, G. Liu, C. Gu, W. Liu, J. Xu, B. Li and W. Wang, *J. Mater. Chem. A*, 2016, **4**, 11630–11634.

7 (*a*) L. Qin, H.-Z. Chen, J. Lei, Y.-Q. Wang, T.-Q. Ye and H.-G. Zheng, *Cryst. Growth Des.*, 2017, **17**, 1293–1298; (*b*) L. L. Liu, C. X. Yu, Y. R. Li, J. J. Han, F. J. Ma and L. F. Ma, *CrystEngComm*, 2015, **17**, 653–664; (*c*) M. L. Hu, S. A. Razavi, M. Piroozzadeh and A. Morsali, *Inorg. Chem. Front.*, 2020, **7**, 1598–1632; (*d*) H. He, L. Hashemi, M.-L. Hu and A. Morsali, *Coord. Chem. Rev.*, 2018, **376**, 319–347; (*e*) J. Liu, W. Wang, Z. Luo, B. Li and D. Yuan, *Inorg. Chem.*, 2017, **56**, 10215–10219.

8 D. Zhao, D. J. Timmons, D. Yuan and C. Zhou, *Acc. Chem. Res.*, 2011, **44**, 123–133.

9 (*a*) J. P. Zhang, Y. B. Zhang, J. B. Lin and X. M. Chen, *Chem. Rev.*, 2012, **112**, 1001–1033; (*b*) H. Deng, S. Grunder, K. E. Cordova, C. Valente, H. Furukawa, M. Hmadeh, F. Gandara, A. C. Whalley, Z. Liu, S. Asahina, H. Kazumori, M. O'Keeffe, O. Terasaki, J. F. Stoddart and O. M. Yaghi, *Science*, 2012, **336**, 1018–1023.

10 (*a*) V. A. Tran, A. N. Kadam and S. W. Lee, *J. Alloys Compd.*, 2020, **835**, 155414; (*b*) W. Liu, L. Liu, C. Lieu, Y. Hao, H. Yang, B. Yuan and J. Jiang, *Biochem. Eng. J.*, 2016, **110**, 115–124.

11 (*a*) M. Z. Wu, J. Y. Shi, P. Y. Chen, L. Tian and J. Chen, *Inorg. Chem.*, 2019, **58**, 3130–3136; (*b*) H. Wang, C. Huang, Y. Han, Z. Shao, H. Hou and Y. Fan, *Dalton Trans.*, 2016, **45**, 7776–7785.

12 G. Aromí, L. A. Barrios, O. Roubeau and P. Gamez, *Coord. Chem. Rev.*, 2011, **255**, 485–546.

13 (*a*) L. J. Zhou, W. H. Deng, Y. L. Wang, G. Xu, S. G. Yin and Q. Y. Liu, *Inorg. Chem.*, 2016, **55**, 6271–6277; (*b*) F. Yang, G. P. Yang, Y. L. Wu, Y. T. Yan, J. Liu, R. C. Gao, W. Y. Zhang and Y. Y. Wang, *J. Coord. Chem.*, 2018, **71**, 2702–2713.

14 G. M. Sheldrick, *Acta Crystallogr., Sect. A: Found. Adv.*, 2015, **71**, 3–8.

15 (*a*) A. D. Becke, *J. Chem. Phys.*, 1993, **98**, 5648–5652; (*b*) C. T. Lee, W. T. Yang and R. G. Parr, *Phys. Rev. B: Condens. Matter Mater. Phys.*, 1988, **37**, 785–789; (*c*) M. J. Frisch, G. W. Trucks, H. B. Schlegel, G. E. Scuseria, M. A. Robb, J. R. Cheeseman, J. A. Montgomery, T. Vreven Jr, K. N. Kudin, J. C. Burant, J. M. Millam, S. S. Iyengar, J. Tomasi, V. Barone, B. Mennucci, M. Cossi, G. Scalmani, N. Rega, G. A. Petersson, H. Nakatsuji, M. Hada, M. Ehara, K. Toyota, R. Fukuda, J. Hasegawa, M. Ishida, T. Nakajima, Y. Honda, O. Kitao, H. Nakai, M. Klene, X. Li, J. E. Knox, H. P. Hratchian, J. B. Cross, V. Bakken, C. Adamo, J. Jaramillo, R. Gomperts, R. E. Stratmann, O. Yazyev,

A. J. Austin, R. Cammi, C. Pomelli, J. W. Ochterski, P. Y. Ayala, K. Morokuma, G. A. Voth, P. Salvador, J. J. Dannenberg, V. G. Zakrzewski, S. Dapprich, A. D. Daniels, M. C. Strain, O. Farkas, D. K. Malick, A. D. Rabuck, K. Raghavachari, J. B. Foresman, J. V. Ortiz, Q. Cui, A. G. Baboul, S. Clifford, J. Cioslowski, B. B. Stefanov, G. Liu, A. Liashenko, P. Piskorz, I. Komaromi, R. L. Martin, D. J. Fox, T. Keith, M. A. Al-Laham, C. Y. Peng, A. Nanayakkara, M. Challacombe, P. M. W. Gill, B. Johnson, W. Chen, W. M. Wong, C. Gonzalez and J. A. Pople, *Gaussian 09 revision B.01*, Gaussian, Inc., Wallingford CT, 2009; (*d*) N. M. O'Boyle, A. L. Tenderholt and K. M. Langner, *J. Comput. Chem.*, 2008, **29**, 839–845.

16 M. A. Spackman and J. J. McKinnon, *CrystEngComm*, 2002, **4**, 378–392.

17 M. A. Spackman and P. G. Byrom, *Chem. Phys. Lett.*, 1997, **267**, 309.

18 J. J. McKinnon, A. S. Mitchell and M. A. Spackman, *Chem.–Eur. J.*, 1998, **4**, 2136–2141.

19 J. J. McKinnon, M. A. Spackman and A. S. Mitchell, *Acta Crystallogr., Sect. B: Struct. Sci.*, 2004, **60**, 627–668.

20 A. L. Rohl, M. Moret, W. Kaminsky, K. Claborn, J. J. McKinnon and B. Kahr, *Cryst. Growth Des.*, 2008, **8**, 4517–4525.

21 A. Parkin, G. Barr, W. Dong, C. J. Gilmore, D. Jayatilaka, J. J. McKinnon, M. A. Spackman and C. C. Wilson, *CrystEngComm*, 2007, **9**, 648–652.

22 S. K. Wolff, D. J. Greenwood, J. J. McKinnon, D. Jayatilaka and M. A. Spackman, *Crystal Explorer 3.1*, University of Western Australia, Perth, Australia, 2012.

23 J. J. Koenderink and A. J. van Doorn, *Image and Vision Computing*, 1992, **10**, 557–564.

24 (*a*) P. Singh, A. Singh, A. Singh, A. K. Singh, G. Kociok-Köhn, A. Alowais, N. A. Y. Abduh, M. Muddassir and A. Kumar, *CrystEngComm*, 2020, **22**, 2049–2059; (*b*) R. Yadav, M. Trivedi, G. Kociok-Köhn, R. Prasad and A. Kumar, *CrystEngComm*, 2015, **17**, 9175–9184; (*c*) A. Kumar, V. Hüch and V. J. Ram, *CrystEngComm*, 2013, **15**, 7019–7030; (*d*) J. He, J. Wang, Q. Xu, X. Wu, A. Dutta, A. Kumar, M. Muddassir, A. Alowais and N. A. Y. Abduh, *New J. Chem.*, 2019, **43**, 13499–13508.

25 (*a*) Z.-J. Li, X.-Y. Li, Y.-T. Yan, L. Hou, W.-Y. Zhang and Y.-Y. Wang, *Cryst. Growth Des.*, 2018, **18**, 2031–2039; (*b*) X. Feng, J. S. Zhao, B. Liu, L. Y. Wang, J. G. Wang, S. W. Ng, G. Zhang, X. G. Shi and Y. Y. Liu, *Cryst. Growth Des.*, 2010, **10**, 1399–1408.

26 (*a*) L. Jin, Q. Liu and W. Sun, *CrystEngComm*, 2014, **16**, 3816–3928; (*b*) X. Feng, B. Liu, L. Y. Wang, J. S. Zhao, J. G. Wang, S. W. Ng and X. G. Shi, *Dalton Trans.*, 2010, **39**, 8038–8049.

27 J. M. Zhou, W. Shi, N. Xu and P. Cheng, *Inorg. Chem.*, 2013, **52**, 8082–8090.

28 A. L. Spek, *J. Appl. Crystallogr.*, 2003, **36**, 7–13.

29 S. Ou, J. P. Zheng, G. Q. Kong and C. D. Wu, *Dalton Trans.*, 2015, **44**, 7862.

30 J.-M. Hu, R. Guo, Y.-G. Liu and G.-H. Cui, *Inorg. Chim. Acta*, 2016, **450**, 418–425.

31 Y. Gong, P. G. Jiang, Y. X. Wang, T. Wu and J. H. Lin, *Dalton Trans.*, 2013, **42**, 7196–7203.

32 F. Wang, Z. S. Liu, H. Yang, Y. X. Tan and J. Zhang, *Angew. Chem., Int. Ed.*, 2011, **50**, 450–453.

33 Z. L. Wu, C. H. Wang, B. Zhao, J. Dong, F. Lu, W. H. Wang, W. C. Wang, G. J. Wu, J. Z. Cui and P. Cheng, *Angew. Chem., Int. Ed.*, 2016, **55**, 4938–4942.

34 F. Wang, Y. Pu, X. Zhang, F. Zhang, H. Cheng and Y. Zhao, *J. Lumin.*, 2019, **206**, 192–198.

35 F. Q. Wang, C. M. Wang and Z. C. Yu, *RSC Adv.*, 2015, **5**, 70086–70093.

36 (*a*) L. L. Wen, J. B. Zhao, K. L. Lv, Y. H. Wu, K. J. Deng, X. K. Leng and D. F. Li, *Cryst. Growth Des.*, 2012, **12**, 1603–1612; (*b*) X. Du, H. He, L. Du, W. Li, Y. Wang, Q. Jiang, L. Yang, J. Zhang and S. Guo, *Polyhedron*, 2019, **171**, 221–227.

37 L. Ding, J.-C. Zhong, X.-T. Qiu, Y.-Q. Sun and Y.-P. Chen, *J. Solid State Chem.*, 2017, **246**, 138–144.

38 C. C. Wang, J.-R. Li, X. L. Lv, Y.-Q. Zhang and G. S. Guo, *Energy Environ. Sci.*, 2014, **7**, 2831–2867.

39 (*a*) J.-J. Wang, P.-P. Si, J. Yang, S.-S. Zhao, P.-P. Li, B. Li, S.-Y. Wang, M. Lu and S.-X. Yu, *Polyhedron*, 2019, **162**, 255–262; (*b*) J. J. Du, Y. P. Yuan, J. X. Sun, F. M. Peng, X. Jiang, L. G. Qiu, A. J. Xie, Y. H. Shen and J. F. Zhu, *J. Hazard. Mater.*, 2011, **190**, 945–951.

40 (*a*) W. Pan, C. H. Gong, X. H. Zeng, C. Y. Hu, Y. Zhang, D. R. Zhu, H. Xu, H. Y. Guo, J. Y. Zhang and J. L. Xie, *Polyhedron*, 2019, **169**, 24–31; (*b*) T. Zhang and W. Lin, *Chem. Soc. Rev.*, 2014, **43**, 5982–5993.